Nanoscale

PAPER

View Article Online
View Journal | View Issue

Cite this: *Nanoscale*, 2025, **17**, 6593

Alternate InP synthesis with aminophosphines: solution–liquid–solid nanowire growth†

Helen C. Larson, [a] Zhixing Lin,[b] François Baneyx [b] and Brandi M. Cossairt [a]*

Received 22nd November 2024,
Accepted 7th February 2025

DOI: 10.1039/d4nr04907a

rsc.li/nanoscale

Indium phosphide nanowires are important components in high-speed electronics and optoelectronics, including photodetectors and photovoltaics. However, most syntheses either use high-temperature and costly vapor-phase methodology or highly toxic and pyrophoric tris(trimethylsilyl)phosphine. To expand on the success of the aminophosphine-based InP colloidal quantum dot synthesis, we developed a synthesis for thin (~11 nm) zinc blende InP nanowires at 180 °C using indium tris(trifluoroacetate) and tris(diethylamino)phosphine. A flat nanoribbon morphology was identified by transmission electron and atomic force microscopy analysis, with the stoichiometric (110) lattice plane exposed. Nanowire growth proceeded through a solution–liquid–solid mechanism from *in situ*-formed indium metal nanoparticles. Molecular byproducts of tris(oleylamino)phosphine oxide and *N*-oleyltrifluoroacetamide observed by ^{31}P and ^{19}F NMR spectroscopy inform a proposed mechanism of indium reduction by the aminophosphine. Morphological control over the nanowire product was achieved by varying the phosphorus injection to control the aspect ratio, the In : P ratio to toggle between nanowires and multipods, and the pre-hot injection evacuation step to favor a quantum dot product. Replacing the indium precursor with indium tris(trifluoromethanesulfonate) was found to make bulk zinc blende InP nanowires with an average diameter of >250 nm and tens of microns in length.

Introduction

Indium phosphide is a high-performing semiconductor found in many current and emerging technologies. The relatively large, direct bandgap of 1.34 eV and high carrier mobilities, in particular, elevate InP above other semiconductors for use in high-speed electronics, such as heterojunction bipolar transistors and high-electron-mobility transistors, and optoelectronics, such as single-photon detectors and extraterrestrial photovoltaics.[1–5] Beyond the bulk, InP nanowires are unique building blocks for electronic and optoelectronic devices due to additional properties like confined carrier transport in one dimension and a tunable band gap.[1,6,7] For example, InP nanowires have a large polarization sensitivity helpful for photodetection and are amenable to hybrid fabrication, which enable complex device architectures such as avalanche photodetectors and dot-in-wire telecom emission devices.[1,8,9] Additionally, InP nanowires can be doped and assembled to build precise electronic or optoelectronic devices, as demonstrated by an electroluminescent p–n junction made of crossed InP nanowires from Lieber and coworkers.[10]

Colloidal synthesis is a potential path to scalable InP nanowire growth. Solution-phase growth is more cost-effective, uses less substrate, and operates at lower temperatures than vapor-phase nanowire manufacturing techniques.[2,11] Solution–liquid–solid (SLS) growth is a nanowire growth mechanism that achieves anisotropy by confining nucleation and growth within a colloidally dispersed liquid metal nanodroplet.[12,13] The precursors diffuse from solution into the metal droplet, nucleate, and grow in one dimension constrained by the droplet interface. Buhro and coworkers discovered the SLS mechanism in 1995 as a solution phase analog of vapor–liquid–solid nanowire growth, which gave rise to a broad investigation of SLS nanowire growth of many compositions.[12,14] There were rapid developments in SLS-grown InP nanowires throughout the 2000s, including improvements in diameter by controlling the metal nanoparticle size,[15–18] length control by tuning precursor to metal nanoparticle ratios,[7,19,20] optical properties,[21] and self-seeded SLS.[22,23] However, the majority of SLS InP nanowire syntheses use pyrophoric, highly-toxic tris(trimethylsilyl)phosphine, with a limited number of syntheses using other phosphorus precursors such as trioctylphosphine[24] or solid hydrogen phosphide.[25] There remains a need

[a]*Department of Chemistry, University of Washington, Seattle, WA 98195, USA. E-mail: cossairt@uw.edu*
[b]*Department of Chemical Engineering, University of Washington, Seattle, WA 98195, USA*

†Electronic supplementary information (ESI) available: Additional spectroscopic, microscopic, and analytical data is available in Fig. S1–S21. See DOI: https://doi.org/10.1039/d4nr04907a

to investigate alternate phosphorus precursors to access InP nanowire synthesis that avoids tris(trimethylsilyl)phosphine.[1,2]

Direct colloidal nucleation of anisotropic InP remains elusive.[26,27] Typical colloidal synthesis uses tris(trimethylsilyl) phosphine and an indium carboxylate, and proceeds through a kinetically stable magic-sized cluster intermediate to achieve high-quality InP quantum dots (QDs).[26,28,29] The resulting nanocrystals are quasi-spherical, with an indium-rich surface passivated by carboxylate ligands. Shapes other than spheres and tetrahedra have not been achieved.[26] Dümbgen and co-workers proposed that this is due to the inability of anionic ligands to adequately charge balance surface indium on facets such as (100), which is required for elongated nanocrystals.[27] The alternate InP chemistry based on aminophosphines, a non-pyrophoric, less hazardous phosphorus precursor, produces halide- and amine-capped tetrahedral QDs.[30–33] The aminophosphine-based synthesis has proved to be a versatile system for tuning reaction kinetics as it follows temperature-dependent continuous or burst nucleation and avoids the kinetic trap of the magic-sized cluster.[34–36] As in InP QD synthesis, aminophosphine is a great candidate for expanding the SLS phosphorus precursor chemistry. To our knowledge, the only example of InP nanowire synthesis through the SLS growth mechanism using aminophosphine is an electrically controlled nanowire synthesis using InI_3 and aminophosphine, where the metal catalyst particles were anchored to a solid electrode support.[37] Another lower-toxicity phosphorus precursor, trioctylphosphine, has been used to make InP nanowires through SLS, where trimethylindium decomposes into indium metal, which catalyzes trioctylphosphine decomposition.[24]

In this study, we report the colloidal synthesis of approximately 11 nm diameter InP nanowires from tris(diethyl)aminophosphine and indium tris(trifluoroacetate) in oleylamine. The nanowires were characterized by transmission electron microscopy (TEM) and atomic force microscopy (AFM), revealing a flat, nanoribbon morphology. Microscopy analysis and powder X-ray diffraction (PXRD) identified indium metal on the nanowire tip, pointing toward an SLS growth mechanism. The mechanism of indium metal formation was investigated with nuclear magnetic resonance (NMR) spectroscopy and was found to depend on the interaction of aminophosphine and the indium precursor. We observed variations in the morphology of the aminophosphine-based nanowires dependent on the reaction conditions, including length control, multipod formation, and QD formation. Microns-long bulk InP nanowires were formed using an alternate indium precursor, indium tris(trifluoromethanesulfonate). We present this aminophosphine-based SLS InP nanowire synthesis as a versatile method to access colloidal anisotropic InP that does not rely on the use of tris(trimethylsilyl)phosphine.

Results and discussion

Synthesis of InP nanowires

InP nanowires were prepared from indium tris(trifluoroacetate) ($In(TFA)_3$) and tris(diethylamino)phosphine ($P(NEt_2)_3$). The nanowire synthesis conditions were adapted from aminophosphine-based InP QD synthesis by choosing a weakly binding indium–carboxylate pair.[31] $In(TFA)_3$ was made using a modified literature procedure by refluxing indium metal and neat trifluoroacetic acid.[38] A ^{19}F NMR spectrum containing a single peak at −75.8 ppm in toluene-d_8 was obtained, and a mass spectrum was collected in methanol showing monomeric and dimeric indium-trifluoroacetate species (Fig. S1†). To synthesize InP nanowires, $In(TFA)_3$ in oleylamine was heated under vacuum at 120 °C for one hour, followed by hot injection of aminophosphine at the reaction temperature of 180 °C (Scheme 1). TEM analysis revealed the main reaction product to be InP nanowires, approximately 11 nm in diameter, with an average size dispersion of 50% across several replicate syntheses, with a length of hundreds of nanometers to microns (Fig. 1a).

Looking closer at some of the larger diameter nanowires with TEM, there is a stripe pattern reminiscent of the thin layer buckling of nanobelts reported in the literature (Fig. 1b).[39] The fast Fourier transform of the lattice showed a single crystalline lattice, ruling out the possibility that the stripe pattern is from stacking faults (Fig. S2†). AFM was employed to measure the height of these larger diameter (~100 nm) structures and found the height to be around 10–30 nm, with an average width-to-height ratio of 4 (Fig. 1e and Fig. S3†). Therefore, we can more accurately describe these nanowires as nanoribbons, a subclass of nanowires that are flat. This is interesting because anisotropy is unusual for InP nanocrystals, as discussed in the introduction. In the SLS literature for other crystal compositions, a nanoribbon morphology has been described and arises from favorable stabilization of flat facets during nanowire growth by surfactants.[40,41]

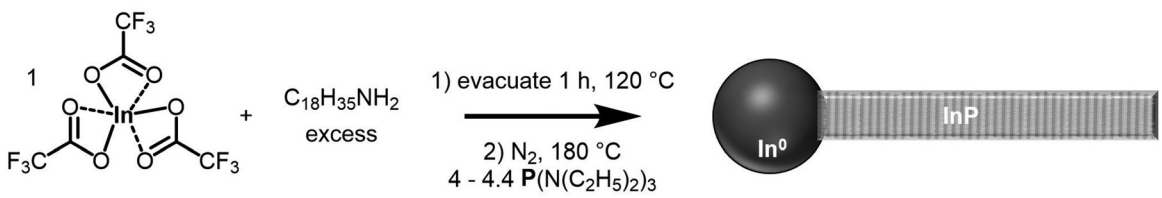

Scheme 1 InP nanowire synthesis from indium tris(trifluoroacetate) and tris(diethylamino)phosphine in oleylamine, proceeding through the solution–liquid–solid growth mechanism.

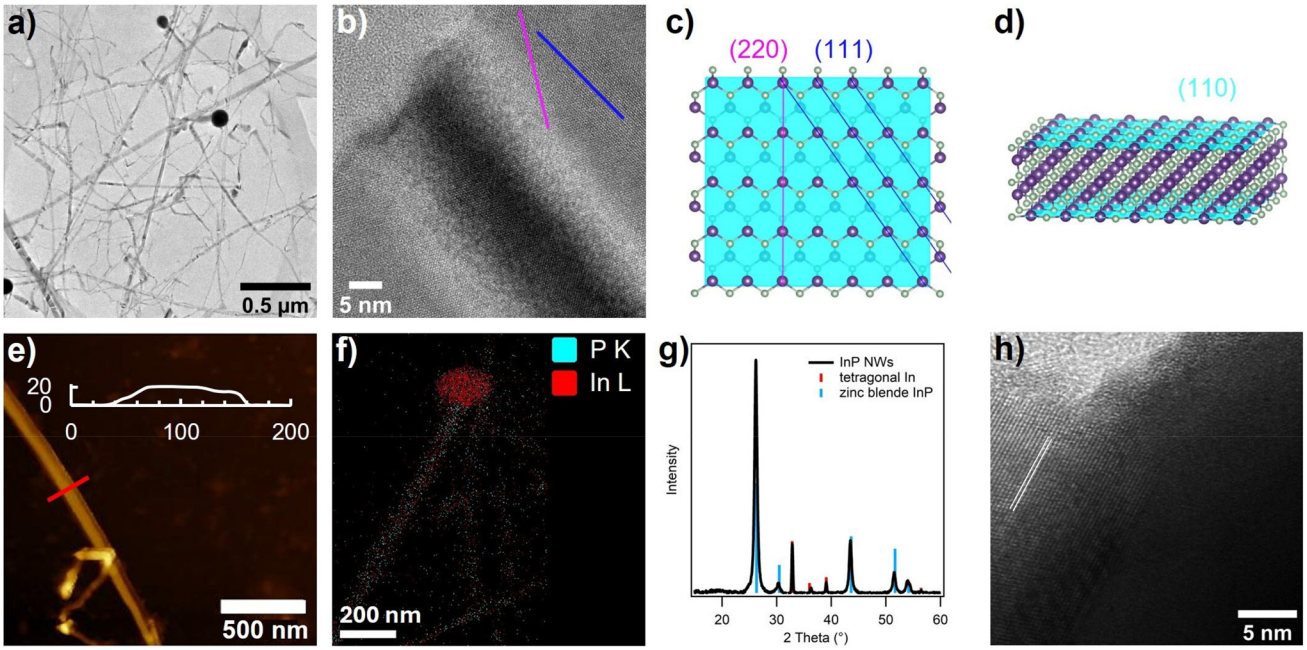

Fig. 1 (a) TEM image of InP nanowires with indium particles observed on some nanowire ends. (b) TEM image of a nanoribbon buckling pattern in a continuous InP zinc blende lattice, with the (111) (dark blue) and (220) (pink) lattice planes marked. Views of the InP zinc blende lattice (c) matching the crystallographic orientation of (b), and (d) showing the stoichiometric (110) lattice plane in light blue. (e) AFM image of an InP nanoribbon with the inset showing height (nm) profile along the red line. (f) STEM EDS map showing indium located at the particle tip with both indium and phosphorus located along the nanowire. (g) PXRD pattern of the purified reaction product revealing a zinc blende InP crystallite size of 16.4 ± 1.4 nm, and large tetragonal indium metal. (h) High-resolution TEM image of InP nanowire/In metal interface (white lines show 111 lattice planes, d = 0.34 nm).

With this in mind, the top facet of the nanoribbons is (110), identified as it is perpendicular to two facets observed in the TEM image, (111) and (220) (Fig. 1b–d). The (110) facet is stoichiometric, unlike the cation-rich basal facets observed in cadmium chalcogenide nanoplatelets.[42–45] This makes sense as the cadmium chalcogenide nanoplatelets are synthesized with strongly coordinating acetate and fatty acids, whereas the InP nanoribbons are prepared in a bath of oleylamine with trifluoroacetate as the only potential X-type ligand. Since trifluoroacetate is a weak Lewis base, observing a stoichiometric basal plane with only L-type ligand passivation is well rationalized. Previously reported SLS-grown InP nanowire syntheses do not discuss a nanoribbon structure, although similar buckling can be noted occasionally in the published TEM images.[7,13–25,37] A (110) facet is also observed on the surface of InP nanoneedles made with trioctylphosphine as the phosphorus precursor.[24]

Spherical nanoparticles of high contrast were observed on the tips of some of the nanowires by TEM. Scanning TEM energy dispersive X-ray spectroscopy (STEM-EDS) revealed that these nanoparticle tips are primarily indium, while both indium and phosphorus are found localized on the nanowire (Fig. 1f). This agrees with the PXRD pattern of the nanowires, which showed both zinc blende InP with an average crystallite size of 16.6 ± 1.4 nm and tetragonal indium metal present in the isolated reaction product (Fig. 1g). Zooming in on the interface between the indium nanoparticle and the InP nanowire, high-resolution TEM imaging revealed the zinc blende InP lattice emerging from the indium metal, with lattice fringes showing that growth occurs along [111] (Fig. 1h). The presence of indium metal nanoparticles at the tip of nanowires points toward the SLS mechanism for nanowire growth, where the indium nanoparticles are presumably formed *in situ* and then act as catalyzing 'nanoreactors' to propel the growth of the nanowires. Pre-made indium metal nanoparticles can also be used to grow InP nanowires from the aminophosphine precursor, either in addition to or instead of the indium precursor (Fig. S4†).

UV-visible absorbance spectra collected over the course of the reaction initially show only a slight absorbance intensity in the high energy region, then an increase in scattering is observed around 10–15 minutes (Fig. S5a†). This is attributed to initial precursor species and oleylamine, then the growth of long, less colloidally stable nanowires. The production of indium metal nanoparticles is hypothesized to occur before the growth of the InP nanowires, as expected following the SLS mechanism.[12] Although InP nanowires with diameters around 11 nm should experience quantum confinement to absorb around 866 nm,[16] clear absorbance peaks are not observed likely due to high polydispersity and scattering, and there is no observable photoluminescence (Fig. S5b†). The peak around 400 nm is attributed to a plasmon resonance of the indium nanoparticles formed in the reaction.[46]

It is interesting to note the continued necessity of the evacuation step at 120 °C to synthesize nanowires. This step was previously included in aminophosphine-based InP QD synthesis to remove water from the hydrophilic indium halide salts. To investigate this, two control syntheses without evacuation were performed. The first control held at 120 °C under nitrogen for one hour, and the second control skipped the 120 °C step and heated straight to the reaction temperature under nitrogen. The UV-vis absorbance spectra of both control syntheses showed a drastic decrease in absorbance and scattering, consistent with a very low concentration of semiconductor in solution, and the TEM images revealed sparse, low-quality indium-InP particles with a tadpole-like morphology (Fig. S6†). The evacuation step appears to have a significant impact on the nanowire yield. Diffusion-ordered ^{19}F NMR spectroscopy of the reaction precursor mixture with and without the evacuation step shows a minor difference in the $In(TFA)_3$ diffusion coefficients consistent with an increase in the solubilization of the precursor (Fig. S7†). Therefore, the evacuation step likely contributes to nanowire formation by increasing the concentration of $In(TFA)_3$ in solution available to form indium metal nanoparticles.

The concentration of precursors was also investigated as a synthetic parameter. A lower overall reaction concentration was initially hypothesized to improve nanowire diameter dispersity as it could limit the coalescence of the indium nanoparticles after formation and decrease the resulting polydispersity. A nanowire synthesis with 0.03 M $In(TFA)_3$ (opposed to 0.06 M for standard conditions) does produce nanowires; however, the average nanowire diameter increases to 37 nm, and the sample maintains a high dispersity of 115% (Fig. S8†). Therefore, a higher indium precursor concentration is useful to access more monodisperse nanowires, potentially due to accelerated nanowire nucleation kinetics outcompeting coalescence of the indium nanoparticles.

Mechanism of indium reduction

The SLS mechanism of colloidal nanowire growth is well-studied in the literature,[12] and the key to accessing SLS growth is the presence of catalytic metal nanoparticles. Therefore, we investigated the production of indium metal in our synthesis by assessing potential reducing agents for $In(TFA)_3$ (Scheme 2). The most obvious candidate for the indium reducing agent was the solvent oleylamine, known to act as a reducing agent in some nanocrystal syntheses.[47–50] To test if oleylamine reduces $In(TFA)_3$ to indium metal, a control reaction was run identical to the nanowire reaction described in Scheme 1 except without the aminophosphine injection. The product was nanocrystalline indium oxide by PXRD, and TEM showed a lack of the large, tens to hundreds of nanometers in diameter indium nanoparticles observed in the nanowire reaction (Fig. S9†). Under these reaction conditions, oleylamine does not reduce indium to the extent seen when aminophosphine is present. This control reaction mimicked the nanowire reaction conditions until the hot injection of the aminophosphine, suggesting that $P(NEt_2)_3$ is necessary for the indium reduction. Diethylamine is released from $P(NEt_2)_3$ when it undergoes transamination with oleylamine and generally, secondary amines are stronger reducing agents than primary amines. However, a similar control reaction with the injection of aminophosphine replaced with three equivalents of diethylamine also produced indium oxide instead of indium metal (Fig. S9†). Therefore, we concluded that the indium reducing agent was likely the aminophosphine itself. Aminophosphines are known to be redox active in the indium halide-based InP QD synthesis chemistry, where it reduces itself from P(III) to P(-III) through three subsequent two-electron reduction events.[30,31]

The role of $P(NEt_2)_3$ as the indium reducing agent was investigated through analysis of the molecular byproducts of the nanowire synthesis. The ^{31}P NMR spectrum of the crude nanowire reaction solution revealed only one major phosphorus-containing molecular byproduct, at 18 ppm, which is in the chemical shift range expected for oxidized phosphorus (V) (Fig. 2b).[51] A potential candidate for this byproduct is the aminophosphine oxide of the transaminated $P(NEt_2)_3$, $OP(NHR)_3$ (R = $C_{18}H_{35}$). This can be separately synthesized by adapting a literature method for tris(dimethylamino)phosphine oxide[51] and carrying out transamination with oleylamine[52,53] (Fig. S10 and S11†). The chemical shift of $OP(NHR)_3$ is 20.5 ppm in deuterated toluene; however, when $OP(NHR)_3$ was spiked into a sample of the crude nanowire reaction solution, there were no additional peaks observed except a slight broadening around the peak at 18 ppm (Fig. S12†). This suggests that the major phosphorus-containing molecular byproduct is tris(oleylamino)phosphine oxide, and phosphorus

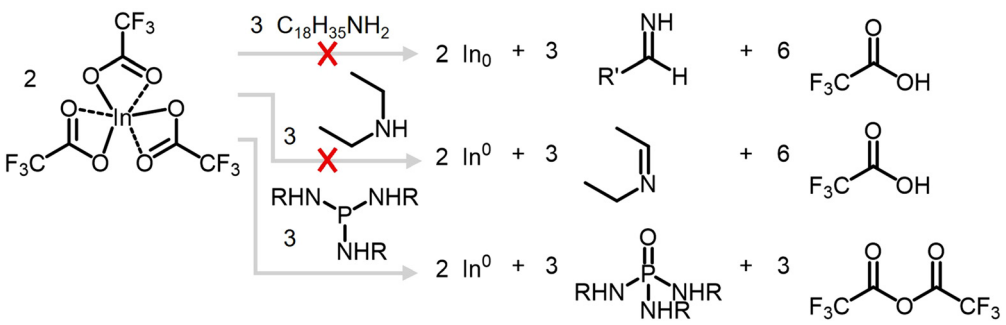

Scheme 2 Options for the reduction of indium (R = $C_{18}H_{35}$, R′ = $C_{17}H_{33}$).

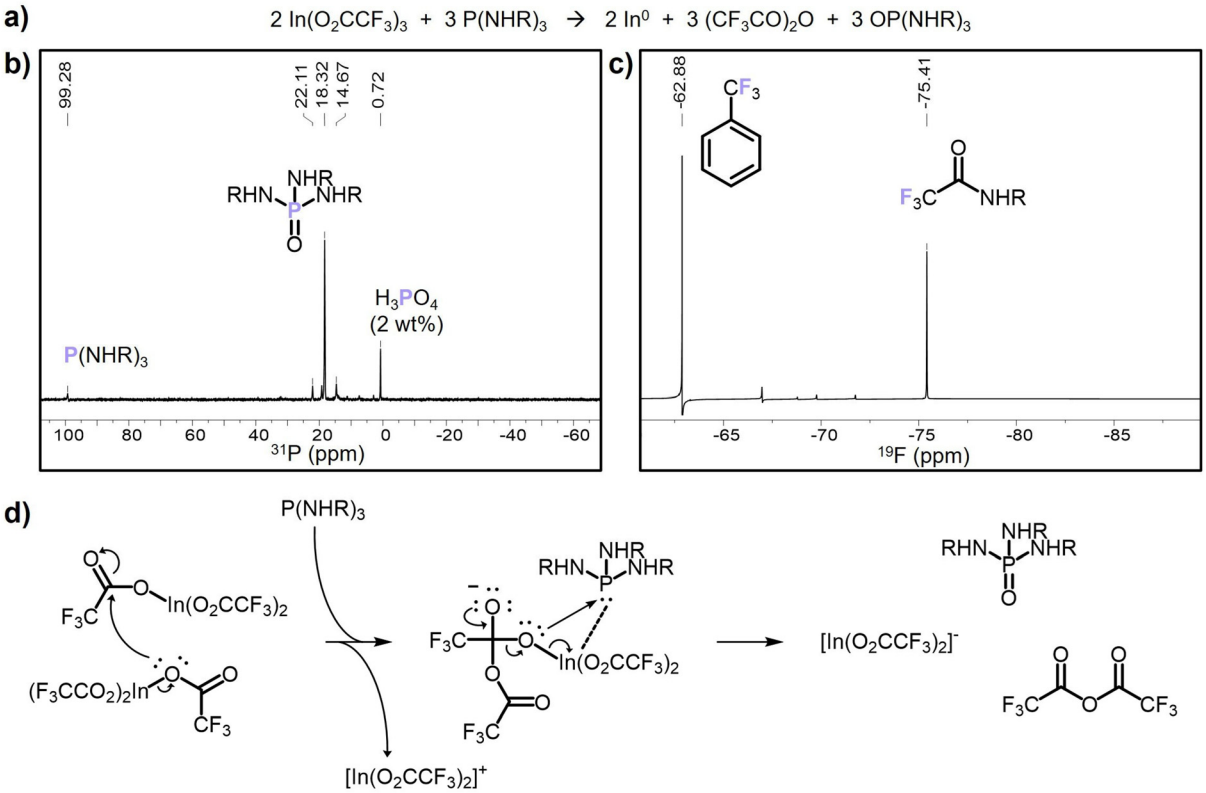

Fig. 2 (a) Balanced reaction equation for the reduction of $In(TFA)_3$ by transaminated aminophosphine. (b) ^{31}P NMR spectrum of the crude nanowire reaction solution with the reaction byproduct identified as tris(oleylamino)phosphine oxide, starting material $P(NHR)_3$, and a 2 weight% H_3PO_4 capillary reference (202 MHz, toluene-d_8, DS 2, NS 40, D1 10 s). (c) ^{19}F NMR spectrum of the crude nanowire reaction solution with the reaction byproduct identified as *N*-oleyltrifluoroacetamide and a trifluorotoluene capillary reference (470 MHz, toluene-d8, DS 2, NS 40, D1 10 s). (d) Proposed mechanism for indium reduction: concerted indium reduction and sacrificial phosphorus oxidation (R = $C_{18}H_{35}$).

oxidation from (III) to (V) is likely the source of electrons to reduce In^{3+}.

The second clue to the indium reduction mechanism came from tracking the trifluoroacetate moiety of the indium precursor. The ^{19}F NMR spectrum of the crude nanowire reaction solution contained a single peak at −75.5 ppm, indicating one major fluorine-containing molecular byproduct (Fig. 2c). This is in the chemical shift region for trifluoroacetic anhydride and does not match with either $In(TFA)_3$ (−75.8 ppm) or trifluoroacetic acid (−75.9 ppm) (Fig. S13†). If trifluoroacetic anhydride was produced during the indium reduction reaction, it is expected to continue to react with the solvent, oleylamine, through an aminolysis reaction to form *N*-oleyltrifluoroacetamide.[54] A separate reaction between oleylamine and trifluoroacetic anhydride at the nanowire reaction temperature of 180 °C to produce *N*-oleyltrifluoroacetamide matches the chemical shift of the observed fluorine-containing byproduct (Fig. S14†). Therefore, trifluoroacetic anhydride as a byproduct of the indium reduction is reasonable, and expected from a balanced reaction equation (Fig. 2a).

Considering the observed molecular byproducts of tris(oleylamino)phosphine oxide and *N*-oleyltrifluoroacetamide, we propose that the initial step of indium reduction occurs *via* the mechanism shown in Fig. 2d. Two equivalents of $In(TFA)_3$ participate in a nucleophilic attack between two of the trifluoroacetate moieties to begin forming the trifluoroacetic anhydride, followed by reductive elimination of the indium-oxygen bond and concerted oxygen atom transfer to the aminophosphine releasing an indium(I) bis(trifluoroacetate) complex, tris(oleylamino)phosphine oxide, and trifluoroacetic anhydride. Further indium reduction is expected to occur *via* a similar pathway. In this mechanism, the electrophilicity of the carbonyl carbon in the trifluoroacetate groups drives the chemistry.

It is interesting to note that nanowires and the preceding indium metal nanoparticles have not been observed in aminophosphine-based InP QD syntheses from indium(III) halides. To confirm this, quantum dot syntheses were run with either $InCl_3$ or InI_3 as the indium precursor instead of $In(TFA)_3$, and the same purification procedure was applied as for the $In(TFA)_3$-nanowires to isolate any large colloidally unstable nanowire or indium metal products. The PXRD pattern of the resulting product revealed small InP QDs and a large peak likely related to organics around 20 degrees two theta and no indium metal (Fig. S15†). We investigated the reduction potentials of $InCl_3$, InI_3, and $In(TFA)_3$ in acetonitrile using cyclic voltammetry and observed features consistent with a nucleation

loop, where there is higher current density on the reverse scan that represents electrodeposition of, in this case, indium metal (Fig. S16†).[55] Both InI_3 and $InCl_3$ were easier to reduce than $In(TFA)_3$, therefore we believe that the above mechanism, which highlights the importance of the reactive carbonyl chemistry, is a better explanation for the formation of indium metal.

Morphology control

Through modifications of the indium precursor, the phosphorus equivalents and addition rate, or the evacuation step, the aminophosphine-$In(TFA)_3$ chemistry can access a multipod morphology, lower aspect ratio nanoplates, QDs, and large, bulk InP nanowires. The multipod morphology is when multiple nanowires emerge from a single metal catalyst particle. We observed multipods as the predominant synthesis product under two conditions related to the purity of the indium precursor and the ratio of indium to phosphorus. First, multipods were observed when the $In(TFA)_3$ precursor contained excess trifluoroacetic acid (Fig. S17a and b†). This is supported by a control experiment where 0.1 equivalent trifluoroacetic acid is added back into pure $In(TFA)_3$, and similar multipods and shortened nanowires were observed (Fig. S17c†). Second, even with a pure $In(TFA)_3$ precursor, the standard synthesis conditions occasionally produced multipods (Fig. S17d and e†). This reproducibility issue was solved by increasing the phosphorus equivalents from 4 to 4.4 per indium, which reliably produced long InP nanowires with an average diameter of 11 nm (Fig. S18†). Multiple nanowires growing from a single metal particle in SLS has been observed previously in InP nanowire literature and is attributed to either coalescence of the metallic tips of already-grown nanowires,[13,56] or differences in the solubility[57] or chemical potential[58,59] of the component atoms as they diffuse into the liquid metal. Additionally, when the metal particle is solid instead of liquid (solution–solid–solid growth), it can become favorable for multiple arms to nucleate off one particle.[60,61] However, the latter case is not likely to occur in this study because the melting point of indium is well below the reaction temperature, especially considering the size-dependent melting point depression of nanoscale indium.[62]

Adding additional aminophosphine is found to further control the InP morphology towards novel low aspect ratio anisotropic nanocrystals. The metal nanoparticle formation rate and the phosphorus chemical potential (in solution and dissolved in the liquid metal) affect the length of the nanowires, as found previously in SLS InP nanowire literature.[7,12,15,20] However, in this chemistry, the aminophosphine acts both as the phosphorus precursor and the indium-reducing agent, so the exact metal nanoparticle to precursor ratio cannot be easily controlled. Therefore, we investigated the effects of adding additional aminophosphine into the reaction while the nanowires formed. A slow injection at 0.02 mL min^{-1} of an additional 10 mole percent $P(NEt_2)_3$ starting 15 minutes after the initial hot injection resulted in shortening of the nanowire length and formation of rectangular nanoplate-like structures (Fig. 3a and b). Increasing the amount of extra aminophosphine to 50 mole percent while maintaining the rate did not continue to shorten the aspect ratio, instead forming nanowires with wide triangular areas and irregular diameters (Fig. 3c and d). Nanowire length is controlled by balancing the ratio of metal catalyst particles to precursors available for growth.[12] More catalyst nanoparticles lead to shorter nanowires while more precursors lead to longer nanowires. Therefore, the addition of 10 mol% aminophosphine appears to go primarily towards making indium metal because shorter, wider nanowires are observed, while the addition of 50 mol% appears to get used primarily as a nanowire precursor because longer nanowires are observed. It is interesting to find the anisotropy of the width and height in addition to the expected one-dimensional nanowire anisotropy of SLS growth. As discussed in the introduction, the surfaces of zinc blende indium phosphide are not energetically favorable to take on a nanoplate or nanorod morphology.[27] SLS is a method to coax InP into anisotropic morphologies largely inaccessible by traditional colloidal nanocrystal nucleation and growth.

The InP nanowire synthesis using aminophosphines can be expanded to another weakly-binding indium complex, indium tris(trifluoromethanesulfonate) ($In(OTf)_3$). Trifluoromethanesulfonate was chosen to explore the extreme limit of weak indium-ligand coordination.[63] When $In(OTf)_3$ is used as the indium precursor replacing $In(TFA)_3$, much larger bulk InP nanowires are formed, as observed with Scanning Electron Microscopy (SEM) and TEM (Fig. 4a, b, d and f). These nanowires have an average diameter of 272 ± 144 nm, are 10s of microns in length, and the PXRD pattern showed bulk zinc blende InP with a small amount of tetragonal indium metal (Fig. 4c). A large spherical particle was observed occasionally on the end of the large nanowires which SEM-EDS confirmed contains indium and not phosphorus, which suggests a similar SLS growth mechanism to the In$(TFA)_3$-nanowires (Fig. 4e).

In both the syntheses using either $In(TFA)_3$ or $In(OTf)_3$, InP QDs are also formed as a side product. In the reported conditions for the $In(TFA)_3$-based nanowire synthesis, nanowire growth is significantly favored over QD growth, while for In$(OTf)_3$, QD growth is favored. The QDs and the nanowires are separated by centrifugation of the crude reaction solution, where the nanowires crash out and the QDs and other reaction byproducts remain in the oleylamine supernatant. After further purification to isolate the QDs, they were characterized by TEM, PXRD, and NMR spectroscopy. The InP QDs made from $In(TFA)_3$ are zinc blende with a crystallite size of 2.2 ± 0.9 nm by PXRD, and have a lowest energy excitonic transition around 475 nm (Fig. S19a–c†). The QDs made using $In(OTf)_3$ are small and poorly crystalline as evidenced by the broad peaks in the PXRD and the low contrast in the TEM (Fig. S19d–f†). The small size of these QDs is consistent with aminophosphine-based InP reaction kinetics, where an indium halide precursor with a better leaving group produces smaller QDs.[64] The PXRD pattern of these QDs is unique from zinc blende InP and is more reminiscent of a quasi-wurtzite

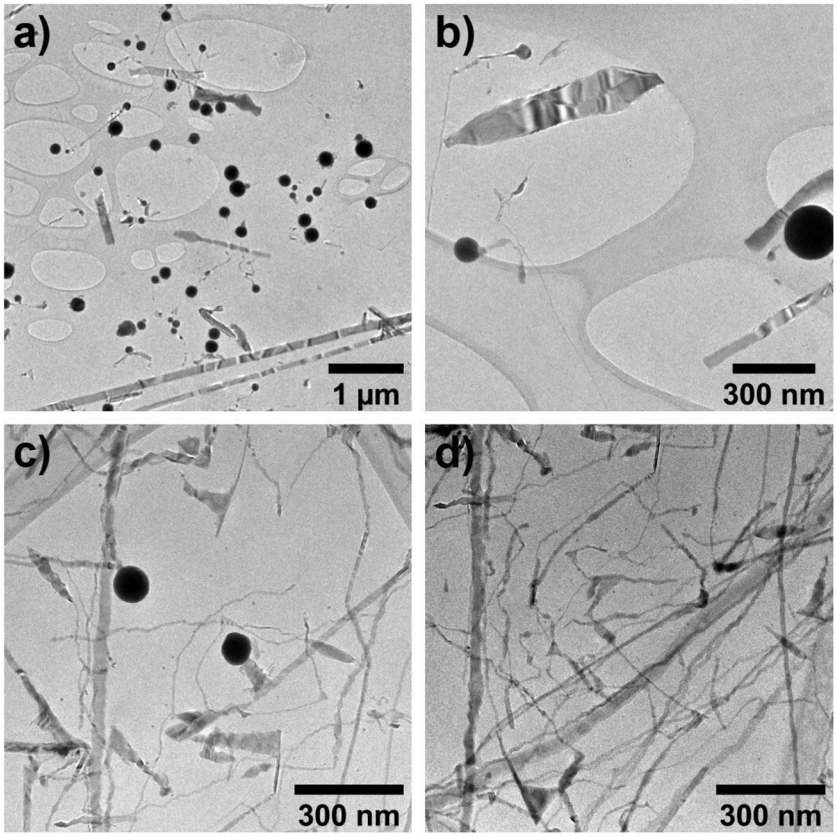

Fig. 3 TEM images of variations on the InP nanowires with 10 (a and b) or 50 (c and d) mole % extra $P(NEt_2)_3$.

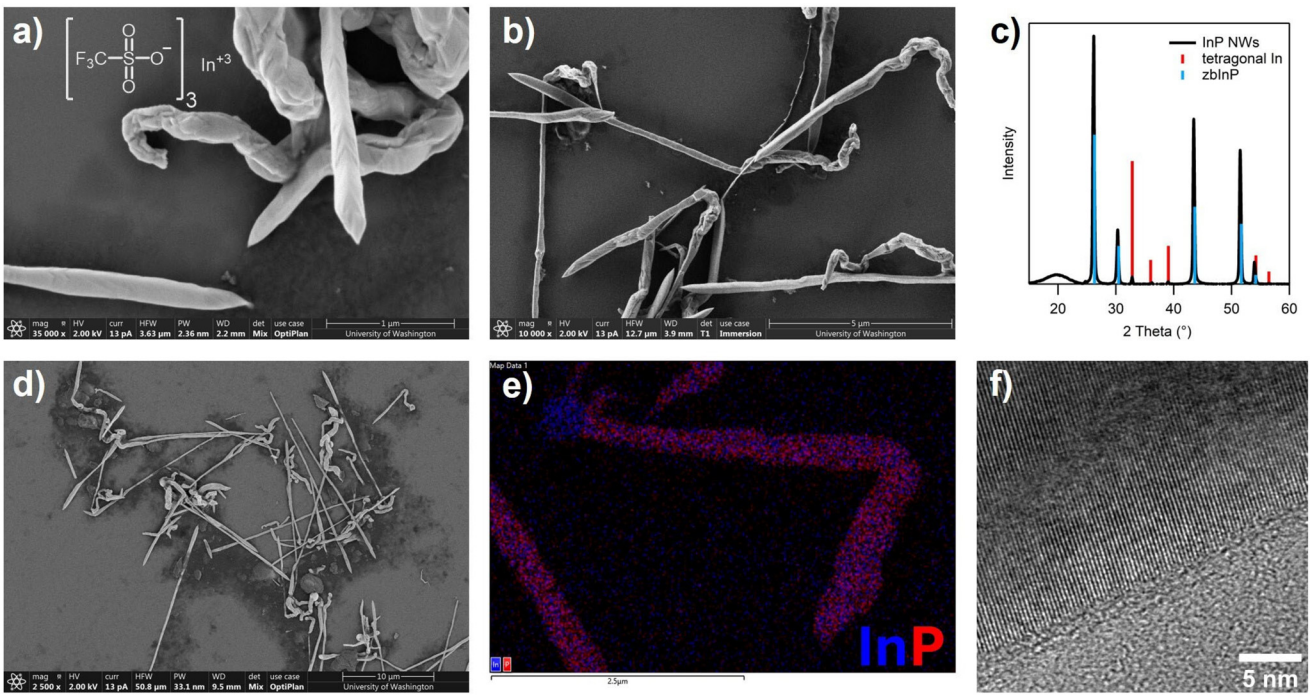

Fig. 4 Characterization of InP nanowires synthesized using $In(OTf)_3$ including SEM images (a, b and d), (c) PXRD pattern showing bulk zinc blende InP and a relatively low amount of tetragonal indium metal, (e) SEM-EDS map showing an InP nanowire growing out of an indium particle, and (f) high-resolution TEM image showing the (111) lattice planes of the edge of a nanowire.

phase also observed in InP magic-sized clusters.[29,65] Looking closer at the QD surface could explain the deviation from the expected zinc blende structure. Typically, aminophosphine-based InP QDs are tetrahedra capped with halides and amines to achieve a perfect mix of X- and L-type ligand binding to passivate the 111 facet.[33] However, switching the indium halide precursor to either $In(TFA)_3$ or $In(OTf)_3$ replaces the halide with a very weakly coordinating organic anion, which is not observed in the QD sample after purification by ^{19}F NMR spectroscopy, only oleylamine is observed on the surface (Fig. S20†). Additionally, by inductively coupled plasma optical emission spectroscopy, these QDs are more stoichiometric (1.1 : 1 In : P) than aminophosphine-based QDs made from indium chloride (1.5 : 1 In : P). This suggests that the QD surface is only passivated by oleylamine, and the lack of a strongly-binding X-type ligand favors the quasi-wurtzite phase over zinc blende.

The QD product was favored over the nanowire product in the synthesis using $In(TFA)_3$ when the evacuation step was skipped. As discussed previously, the nanowire yield decreased with no evacuation step, resulting in more significant QD growth as noted by the prominent QD lowest energy excitonic transition in the UV-vis absorbance spectra (Fig. S6d†). Another condition that favored QDs over nanowires is when the reaction was carried out using a heat-up method rather than an aminophosphine hot injection, which also does not involve the evacuation of $In(TFA)_3$ and oleylamine. Similarly, the UV-vis absorbance spectra over the reaction showed a prominent QD population and an overall low absorbance intensity compared to the hot injection synthesis (Fig. S21†).

Conclusion

We developed a synthesis for InP nanowires using the non-pyrophoric, low-toxicity phosphorus precursor $P(NEt_2)_3$ and $In(TFA)_3$. The nanowires are zinc blende InP, 11 nm in diameter on average, and exhibit a flat, nanoribbon morphology with the stoichiometric (110) facet exposed. These nanowires grow through the SLS mechanism, as evidenced by indium metal nanoparticles on the nanowire tips. The formation of indium nanoparticles occurs *in situ* through the reduction of $In(TFA)_3$ with aminophosphine as the reducing agent. We proposed a mechanism in which two equivalents of $In(TFA)_3$ participate in nucleophilic substitution through the reactive carbonyl, oxygen atom transfer to the aminophosphine, and reductive elimination to yield the initial two-electron reduction of indium, an oxidized aminophosphine oxide, and trifluoroacetic anhydride. We have demonstrated morphology control over the indium nanoparticle-InP nanowire system through modifications to the reactant concentration, injection amount and rate, and the evacuation step to access multipod morphologies, different nanowire lengths, and small InP QDs. Additionally, we expanded the aminophosphine-based SLS chemistry to synthesize bulk InP nanowires from the reaction of $In(OTf)_3$ and $P(NEt_2)_3$.

This study introduces aminophosphine as a suitable phosphorus precursor for colloidal InP nanowire growth. This is important as the industrial relevance of InP and InP nanowires increases, especially while InP nanowire synthesis currently relies on the dangerous, toxic tris(trimethylsilyl)phosphine precursor.[1,66–68] In addition to technological consequence, the anisotropic growth of InP through the SLS mechanism is fundamentally significant to the nanoscale synthesis field because it is a pathway to overcome the synthetic barriers to anisotropic InP nanocrystals. Well-defined InP quantum rods and wires have been achieved through SLS as described in the literature,[7] and our work provides an example of InP nanoribbons and large, rectangular nanoplates. This shows that once the SLS mechanism steers InP into one-dimensional growth, additional width and height anisotropy can arise due to a neutral L-type amine ligand environment. Expanding the SLS mechanism for InP and this aminophosphine-based chemistry will open the possibility of achieving previously implausible anisotropic InP nanocrystals.

Author contributions

Helen C. Larson: synthesis, characterization, investigation, methodology, validation, writing – original draft. Zhixing Lin: AFM measurements. Francois Baneyx: supervision, funding acquisition. Brandi M. Cossairt: supervision, funding acquisition, project administration, writing – review & editing.

Data availability

The data supporting this article have been included in the main text of the manuscript and as part of the ESI.†

Conflicts of interest

There are no conflicts to declare.

Acknowledgements

We are grateful to Micaela K. Homer for the cyclic voltammetry data, Chris Lowe for the mass spectroscopy, and Scott Braswell for assistance with SEM-EDS. This material was based upon work supported by the US Department of Energy, Office of Science, Office of Basic Energy Sciences, as part of the Energy Frontier Research Centers program: CSSAS – The Center for the Science of Synthesis Across Scales under Award Number DE-SC0019288. Part of this work was conducted at the Molecular Analysis Facility, a National Nanotechnology Coordinated Infrastructure (NNCI) site at the University of Washington, which is supported in part by funds from the National Science Foundation (awards NNCI-2025489, NNCI-1542101), the Molecular Engineering & Sciences Institute, and the Clean Energy Institute.

References

1 L.-Q. Yue, Y.-L. Shi, N.-F. Sun, S. Qiang, J.-K. Qin, L. Zhen and C.-Y. Xu, InP Low-Dimensional Nanomaterials for Electronic and Optoelectronic Device Applications: A Review, *Adv. Sens. Res.*, 2023, **2**(10), 2200101, DOI: **10.1002/adsr.202200101**.

2 F. Zafar and A. Iqbal, Indium Phosphide Nanowires and Their Applications in Optoelectronic Devices, *Proc. R. Soc. A*, 2016, **472**(2187), 20150804, DOI: **10.1098/rspa.2015.0804**.

3 C. Mukherjee, M. Deng, V. Nodjiadjim, M. Riet, C. Mismer, D. Guendouz, C. Caillaud, H. Bertin, N. Vaissiere, M. Luisier, X. Wen, M. De Matos, P. Mounaix and C. Maneux, Towards Monolithic Indium Phosphide (InP)-Based Electronic Photonic Technologies for beyond 5G Communication Systems, *Appl. Sci.*, 2021, **11**(5), 2393, DOI: **10.3390/app11052393**.

4 B. Markman and M. Schröter, Indium-Phosphide Transistors: A Review of Current State and Suitability for Commercial > 100 GHz Wireless Communication Systems, *IEEE Microw. Mag.*, 2024, **25**(10), 38–53, DOI: **10.1109/MMM.2024.3428191**.

5 A. K.-W. Chee, On Current Technology for Light Absorber Materials Used in Highly Efficient Industrial Solar Cells, *Renewable Sustainable Energy Rev.*, 2023, **173**, 113027, DOI: **10.1016/j.rser.2022.113027**.

6 I. Mediavilla, J. L. Pura, V. G. Hinojosa, B. Galiana, L. Hrachowina, M. T. Borgström and J. Jimenez, Composition, Optical Resonances, and Doping of InP/InGaP Nanowires for Tandem Solar Cells: A Micro-Raman Analysis, *ACS Nano*, 2024, **18**(14), 10113–10123, DOI: **10.1021/acsnano.3c12973**.

7 F. Wang and W. E. Buhro, Determination of the Rod–Wire Transition Length in Colloidal Indium Phosphide Quantum Rods, *J. Am. Chem. Soc.*, 2007, **129**(46), 14381–14387, DOI: **10.1021/ja075015c**.

8 J. Wang, M. S. Gudiksen, X. Duan, Y. Cui and C. M. Lieber, Highly Polarized Photoluminescence and Photodetection from Single Indium Phosphide Nanowires, *Science*, 2001, **293**(5534), 1455–1457, DOI: **10.1126/science.1062340**.

9 G. Bucci, V. Zannier, F. Rossi, A. Musiał, J. Boniecki, G. Sęk and L. Sorba, Zincblende InAsxP1−x/InP Quantum Dot Nanowires for Telecom Wavelength Emission, *ACS Appl. Mater. Interfaces*, 2024, **16**(20), 26491–26499, DOI: **10.1021/acsami.4c00615**.

10 X. Duan, Y. Huang, Y. Cui, J. Wang and C. M. Lieber, Indium Phosphide Nanowires as Building Blocks for Nanoscale Electronic and Optoelectronic Devices, *Nature*, 2001, **409**(6816), 66–69, DOI: **10.1038/35051047**.

11 M. Fang, N. Han, F. Wang, Z. Yang, S. Yip, G. Dong, J. J. Hou, Y. Chueh and J. C. Ho, III–V Nanowires: Synthesis, Property Manipulations, and Device Applications, *J. Nanomater.*, 2014, **2014**(1), 702859, DOI: **10.1155/2014/702859**.

12 F. Wang, A. Dong and W. E. Buhro, Solution–Liquid–Solid Synthesis, Properties, and Applications of One-Dimensional Colloidal Semiconductor Nanorods and Nanowires, *Chem. Rev.*, 2016, **116**(18), 10888–10933, DOI: **10.1021/acs.chemrev.5b00701**.

13 T. J. Trentler, S. C. Goel, K. M. Hickman, A. M. Viano, M. Y. Chiang, A. M. Beatty, P. C. Gibbons and W. E. Buhro, Solution−Liquid−Solid Growth of Indium Phosphide Fibers from Organometallic Precursors: Elucidation of Molecular and Nonmolecular Components of the Pathway, *J. Am. Chem. Soc.*, 1997, **119**(9), 2172–2181, DOI: **10.1021/ja9640859**.

14 T. J. Trentler, K. M. Hickman, S. C. Goel, A. M. Viano, P. C. Gibbons and W. E. Buhro, Solution-Liquid-Solid Growth of Crystalline III-V Semiconductors: An Analogy to Vapor-Liquid-Solid Growth, *Science*, 1995, **270**(5243), 1791–1794, DOI: **10.1126/science.270.5243.1791**.

15 S. P. Ahrenkiel, O. I. Mićić, A. Miedaner, C. J. Curtis, J. M. Nedeljković and A. J. Nozik, Synthesis and Characterization of Colloidal InP Quantum Rods, *Nano Lett.*, 2003, **3**(6), 833–837, DOI: **10.1021/nl034152e**.

16 H. Yu, J. Li, R. A. Loomis, L.-W. Wang and W. E. Buhro, Two- versus Three-Dimensional Quantum Confinement in Indium Phosphide Wires and Dots, *Nat. Mater.*, 2003, **2**(8), 517–520, DOI: **10.1038/nmat942**.

17 J. M. Nedeljković, O. I. Mićić, S. P. Ahrenkiel, A. Miedaner and A. J. Nozik, Growth of InP Nanostructures via Reaction of Indium Droplets with Phosphide Ions: Synthesis of InP Quantum Rods and InP−TiO2 Composites, *J. Am. Chem. Soc.*, 2004, **126**(8), 2632–2639, DOI: **10.1021/ja039311a**.

18 D. D. Fanfair and B. A. Korgel, Bismuth Nanocrystal-Seeded III-V Semiconductor Nanowire Synthesis, *Cryst. Growth Des.*, 2005, **5**(5), 1971–1976, DOI: **10.1021/cg0502587**.

19 S. Kan, A. Aharoni, T. Mokari and U. Banin, Shape Control of III–V Semiconductor Nanocrystals: Synthesis and Properties of InAs Quantum Rods, *Faraday Discuss.*, 2003, **125**(0), 23–38, DOI: **10.1039/B302898D**.

20 I. Shweky, A. Aharoni, T. Mokari, E. Rothenberg, M. Nadler, I. Popov and U. Banin, Seeded Growth of InP and InAs Quantum Rods Using Indium Acetate and Myristic Acid, *Mater. Sci. Eng., C*, 2006, **26**(5), 788–794, DOI: **10.1016/j.msec.2005.09.040**.

21 F. Wang, H. Yu, J. Li, Q. Hang, D. Zemlyanov, P. C. Gibbons, D. B. Janes and W. E. Buhro, Spectroscopic Properties of Colloidal Indium Phosphide Quantum Wires, *J. Am. Chem. Soc.*, 2007, **129**(46), 14327–14335, DOI: **10.1021/ja074049h**.

22 C.;L. Banerjee, D. Hughes, M. Bochmann and T. Nann, InP Nanowires from Surfactant -Free Thermolysis of Single Molecule Precursors, *Dalton Trans.*, 2012, **41**(24), 7244–7248, DOI: **10.1039/C2DT30283G**.

23 Z. Liu, K. Sun, W.-B. Jian, D. Xu, Y.-F. Lin and J. Fang, Soluble InP and GaP Nanowires: Self-Seeded, Solution–Liquid–Solid Synthesis and Electrical Properties, *Chem. – Eur. J.*, 2009, **15**(18), 4546–4552, DOI: **10.1002/chem.200900190**.

24 T. Strupeit, C. Klinke, A. Kornowski and H. Weller, Synthesis of InP Nanoneedles and Their Use as Schottky

Devices, *ACS Nano*, 2009, **3**(3), 668–672, DOI: 10.1021/nn800846d.

25 T. H. Lim, S. Ravi, C. W. Bumby, P. G. Etchegoin and R. D. Tilley, Synthesis, Characterization and Photoconductivity of Highly Crystalline InP Nanowires Prepared from Solid Hydrogen Phosphide, *J. Mater. Chem.*, 2009, **19**(27), 4852–4856, DOI: 10.1039/B902474C.

26 S. M. Click and S. J. Rosenthal, Synthesis, Surface Chemistry, and Fluorescent Properties of InP Quantum Dots, *Chem. Mater.*, 2023, **35**(3), 822–836, DOI: 10.1021/acs.chemmater.2c03074.

27 K. C. Dümbgen, J. Zito, I. Infante and Z. Hens, Shape, Electronic Structure, and, Trap States in Indium Phosphide Quantum Dots, *Chem. Mater.*, 2021, **33**(17), 6885–6896, DOI: 10.1021/acs.chemmater.1c01795.

28 Y.-H. Won, O. Cho, T. Kim, D.-Y. Chung, T. Kim, H. Chung, H. Jang, J. Lee, D. Kim and E. Jang, Highly Efficient and Stable InP/ZnSe/ZnS Quantum Dot Light-Emitting Diodes, *Nature*, 2019, **575**(7784), 634–638, DOI: 10.1038/s41586-019-1771-5.

29 D. C. Gary, M. W. Terban, S. J. L. Billinge and B. M. Cossairt, Two-Step Nucleation and Growth of InP Quantum Dots via Magic-Sized Cluster Intermediates, *Chem. Mater.*, 2015, **27**(4), 1432–1441, DOI: 10.1021/acs.chemmater.5b00286.

30 M. D. Tessier, K. De Nolf, D. Dupont, D. Sinnaeve, J. De Roo and Z. Hens, Aminophosphines: A Double Role in the Synthesis of Colloidal Indium Phosphide Quantum Dots, *J. Am. Chem. Soc.*, 2016, **138**(18), 5923–5929, DOI: 10.1021/jacs.6b01254.

31 A. Buffard, S. Dreyfuss, B. Nadal, H. Heuclin, X. Xu, G. Patriarche, N. Mézailles and B. Dubertret, Mechanistic Insight and Optimization of InP Nanocrystals Synthesized with Aminophosphines, *Chem. Mater.*, 2016, **28**(16), 5925–5934, DOI: 10.1021/acs.chemmater.6b02456.

32 H. Van Avermaet, P. Schiettecatte, S. Hinz, L. Giordano, F. Ferrari, C. Nayral, F. Delpech, J. Maultzsch, H. Lange and Z. Hens, Full-Spectrum InP-Based Quantum Dots with Near-Unity Photoluminescence Quantum Efficiency, *ACS Nano*, 2022, **16**(6), 9701–9712, DOI: 10.1021/acsnano.2c03138.

33 K. Kim, D. Yoo, H. Choi, S. Tamang, J.-H. Ko, S. Kim, Y.-H. Kim and S. Jeong, Halide–Amine Co-Passivated Indium Phosphide Colloidal Quantum Dots in Tetrahedral Shape, *Angew. Chem.*, 2016, **128**(11), 3778–3782, DOI: 10.1002/ange.201600289.

34 B. M. McMurtry, K. Qian, J. K. Teglasi, A. K. Swarnakar, J. De Roo and J. S. Owen, Continuous Nucleation and Size Dependent Growth Kinetics of Indium Phosphide Nanocrystals, *Chem. Mater.*, 2020, **32**(10), 4358–4368, DOI: 10.1021/acs.chemmater.0c01561.

35 R. Valleix, F. Cisnetti, H. Okuno, P. Boutinaud, G. Chadeyron and D. Boyer, Size-Controlled Indium Phosphide Quantum Dots for Bright and Tunable Light Emission by Simple Hindered Diamine Addition, *ACS Appl. Nano Mater.*, 2021, **4**(10), 11105–11114, DOI: 10.1021/acsanm.1c02577.

36 H. Larson and B. M. Cossairt, Indium–Poly(Carboxylic Acid) Ligand Interactions Modify InP Quantum Dot Nucleation and Growth, *Chem. Mater.*, 2023, **35**(15), 6152–6160, DOI: 10.1021/acs.chemmater.3c01309.

37 A. Dorn, P. M. Allen and M. G. Bawendi, Electrically Controlling and Monitoring InP Nanowire Growth from Solution, *ACS Nano*, 2009, **3**(10), 3260–3265, DOI: 10.1021/nn900820h.

38 P. Sartori, J. Fazekas and J. Schnackers, Wasserfreie trifluoracetate der hauptgruppe III, *J. Fluorine Chem.*, 1972, **1**(4), 463–471, DOI: 10.1016/S0022-1139(00)82967-X.

39 E. H. Massasa, R. Strassberg, A. Vurgaft, Y. Kauffmann, N. Cohen and Y. Bekenstein, Thin Layer Buckling in Perovskite $CsPbBr_3$ Nanobelts, *Nano Lett.*, 2021, **21**(13), 5564–5571, DOI: 10.1021/acs.nanolett.1c00962.

40 F. Wang and W. E. Buhro, Surfactant-Mediated Solution-Liquid–Solid (SLS) Growth of Phase-Pure Wurtzite CdS Quantum Wires, *Chem. Mater.*, 2024, **36**(20), 10307–10318, DOI: 10.1021/acs.chemmater.4c02283.

41 X. Geng, H. Liu, L. Zhai, Z. Xiong, J. Hu, C. Zou, Y. Dong, Y. Yang and S. Huang, Colloidal Synthesis of CuGaS*x*, Se2−*x* Nanoribbons Mediated by Cu1.75(SSe) Nanocrystals as Catalysts, *J. Alloys Compd.*, 2014, **617**, 961–967, DOI: 10.1016/j.jallcom.2014.08.084.

42 S. Singh, R. Tomar, S. ten Brinck, J. De Roo, P. Geiregat, J. C. Martins, I. Infante and Z. Hens, Colloidal CdSe Nanoplatelets, A Model for Surface Chemistry/Optoelectronic Property Relations in Semiconductor Nanocrystals, *J. Am. Chem. Soc.*, 2018, **140**(41), 13292–13300, DOI: 10.1021/jacs.8b07566.

43 S. Ithurria, M. D. Tessier, B. Mahler, R. P. S. M. Lobo, B. Dubertret and A. L. Efros, Colloidal Nanoplatelets with Two-Dimensional Electronic Structure, *Nat. Mater.*, 2011, **10**(12), 936–941, DOI: 10.1038/nmat3145.

44 J. C. van der Bok, P. T. Prins, F. Montanarella, D. N. Maaskant, F. A. Brzesowsky, M. M. van der Sluijs, B. B. V. Salzmann, F. T. Rabouw, A. V. Petukhov, C. De Mello Donega, D. Vanmaekelbergh and A. Meijerink, In Situ Optical and X-Ray Spectroscopy Reveals Evolution toward Mature CdSe Nanoplatelets by Synergetic Action of Myristate and Acetate Ligands, *J. Am. Chem. Soc.*, 2022, **144**(18), 8096–8105, DOI: 10.1021/jacs.2c00423.

45 Z. Li and X. Peng, Size/Shape-Controlled Synthesis of Colloidal CdSe Quantum Disks: Ligand and Temperature Effects, *J. Am. Chem. Soc.*, 2011, **133**(17), 6578–6586, DOI: 10.1021/ja108145c.

46 N. H. Chou, X. Ke, P. Schiffer and R. E. Schaak, Room-Temperature Chemical Synthesis of Shape-Controlled Indium Nanoparticles, *J. Am. Chem. Soc.*, 2008, **130**(26), 8140–8141, DOI: 10.1021/ja801949c.

47 Q. Liu, W. Lu, A. Ma, J. Tang, J. Lin and J. Fang, Study of Quasi-Monodisperse In2O3 Nanocrystals: Synthesis and Optical Determination, *J. Am. Chem. Soc.*, 2005, **127**(15), 5276–5277, DOI: 10.1021/ja042550t.

48 K. M. Nam, J. H. Shim, H. Ki, S.-I. Choi, G. Lee, J. K. Jang, Y. Jo, M.-H. Jung, H. Song and J. T. Park, Single-Crystalline Hollow Face-Centered-Cubic Cobalt Nanoparticles from Solid Face-Centered-Cubic Cobalt Oxide Nanoparticles, *Angew. Chem., Int. Ed.*, 2008, **47**(49), 9504–9508, DOI: **10.1002/anie.200803048**.

49 S. Mourdikoudis and L. M. Liz-Marzán, Oleylamine in Nanoparticle Synthesis, *Chem. Mater.*, 2013, **25**(9), 1465–1476, DOI: **10.1021/cm4000476**.

50 M. A. Airo, S. Gqoba, F.; Otieno, M. J. Moloto and N. Moloto, Structural Modification and Band-Gap Crossover in Indium Selenide Nanosheets, *RSC Adv.*, 2016, **6**(47), 40777–40784, DOI: **10.1039/C6RA00262E**.

51 B. B. Pavankumar, E. Veerashekhar Goud, R. Selvakumar, S. K. Ashok Kumar, A. Sivaramakrishna, K. Vijayakrishna, C. V. S. Brahmananda Rao, K. N. Sabharwal and P. C. Jha, Function of Substituents in Coordination Behaviour, Thermolysis and Ligand Crossover Reactions of Phosphine Oxides, *RSC Adv.*, 2015, **5**(7), 4727–4736, DOI: **10.1039/C4RA13645D**.

52 K. C. Dümbgen, J. Leemans, V. De Roo, M. Minjauw, C. Detavernier and Z. Hens, Surface Chemistry of InP Quantum Dots, Amine–Halide Co-Passivation, and Binding of Z-Type Ligands, *Chem. Mater.*, 2023, **35**(3), 1037–1046, DOI: **10.1021/acs.chemmater.2c02960**.

53 A. G. Rachkov and A. M. Schimpf, Colloidal Synthesis of Tunable Copper Phosphide Nanocrystals, *Chem. Mater.*, 2021, **33**(4), 1394–1406, DOI: **10.1021/acs.chemmater.0c04460**.

54 E. J. Bourne, S. H. Henry, C. E. M. Tatlow and J. C. Tatlow, 767. Studies of Trifluoroacetic Acid. Part VI. Trifluoroacetyl Derivatives of Amines, *J. Chem. Soc.*, 1952, 4014–4019, DOI: **10.1039/JR9520004014**.

55 M. Hu, Y. Wang, Z. Chen, S. Ning and Y. Wei, Study of Indium Electrodeposition and Nucleation Mechanism in Acidic Solution Using EQCM, *Electrochim. Acta*, 2023, **443**, 141963, DOI: **10.1016/j.electacta.2023.141963**.

56 N. S. Karan, Y. Chen, Z. Liu and R. Beaulac, Solution–Liquid–Solid Approach to Colloidal Indium Nitride Nanoparticles from Simple Alkylamide Precursors, *Chem. Mater.*, 2016, **28**(16), 5601–5605, DOI: **10.1021/acs.chemmater.6b02417**.

57 M.-S. Kim and Y.-M. Sung, Successive Solution–Liquid–Solid (SLS) Growth of Heterogeneous Nanowires, *Chem. Mater.*, 2013, **25**(21), 4156–4164, DOI: **10.1021/cm4015018**.

58 N. Kapuria, S. Imtiaz, A. Sankaran, H. Geaney, T. Kennedy, S. Singh and K. M. Ryan, Multipod Bi(Cu2-xS)n Nanocrystals Formed by Dynamic Cation–Ligand Complexation and Their Use as Anodes for Potassium-Ion Batteries, *Nano Lett.*, 2022, **22**(24), 10120–10127, DOI: **10.1021/acs.nanolett.2c03933**.

59 G. Jia and J. Du, Foreign Metal Ions to Control the Morphology of Solution–Liquid–Solid Reaction, *Cryst. Growth Des.*, 2018, **18**(12), 7489–7495, DOI: **10.1021/acs.cgd.8b01289**.

60 K.-T. Yong, Y. Sahoo, M. T. Swihart and P. N. Prasad, Growth of CdSe Quantum Rods and Multipods Seeded by Noble-Metal Nanoparticles, *Adv. Mater.*, 2006, **18**(15), 1978–1982, DOI: **10.1002/adma.200600368**.

61 F. Wang and W. E. Buhro, Crystal-Phase Control by Solution–Solid–Solid Growth of II–VI Quantum Wires, *Nano Lett.*, 2016, **16**(2), 889–894, DOI: **10.1021/acs.nanolett.5b03628**.

62 M. Zhang, M. Y. Efremov, F. Schiettekatte, E. A. Olson, A. T. Kwan, S. L. Lai, T. Wisleder, J. E. Greene and L. H. Allen, Size-Dependent Melting Point Depression of Nanostructures: Nanocalorimetric Measurements, *Phys. Rev. B:Condens. Matter Mater. Phys.*, 2000, **62**(15), 10548–10557, DOI: **10.1103/PhysRevB.62.10548**.

63 N. E. Dixon, G. A. Lawrance, P. A. Lay, A. M. Sargeson and H. Taube, Trifluoromethanesulfonates and Trifluoromethanesulfonato-O Complexes, in *Inorganic Syntheses*, John Wiley & Sons, Ltd, 1990, pp. 70–76. DOI: **10.1002/9780470132593.ch16**.

64 M. D. Tessier, D. Dupont, K. De Nolf, J. De Roo and Z. Hens, Economic and Size-Tunable Synthesis of InP/ZnE (E = S, Se) Colloidal Quantum Dots, *Chem. Mater.*, 2015, **27**(13), 4893–4898, DOI: **10.1021/acs.chemmater.5b02138**.

65 A. Ritchhart and B. M. Cossairt, Templated Growth of InP Nanocrystals with a Polytwistane Structure, *Angew. Chem., Int. Ed.*, 2018, **57**(7), 1908–1912, DOI: **10.1002/anie.201711539**.

66 S. Research, Indium Phosphide Wafer Market Size And Share Report, 2032. **https://straitsresearch.com/report/indium-phosphide-wafer-market** (accessed 2024-11-11).

67 J. Liu, H. Nie, B. Yan, K. Yang, H. Yang, V. Khayrudinov, H. Lipsanen, B. Zhang and J. He, Nonlinear Optical Absorption Properties of InP Nanowires and Applications as a Saturable Absorber, *Photon. Res.*, 2020, **8**(6), 1035–1041, DOI: **10.1364/PRJ.389669**.

68 Targeting telecoms with nanowires - News. Compound Semiconductor. **https://compoundsemiconductor.net/article-gen/112937** (accessed 2024-11-11).